Electronic Supplementary Material (ESI) for Physical Chemistry Chemical Physics.

Supplementary Information for

A comparative study on the reactivity of ditantalum deuteride cluster anions $Ta_2D_2^-$ and $Ta_2D_4^-$ toward N_2

Xin Cheng,[abc] Zi-Yu Li,*[ac] Li-Hui Mou,[abc] Qing-Yu Liu,[ac] and Sheng-Gui He*[abc]

[a] State Key Laboratory for Structural Chemistry of Unstable and Stable Species, Institute of Chemistry, Chinese Academy of Sciences, Beijing 100190, P. R. China

[b] University of Chinese Academy of Sciences, Beijing 100049, P. R. China

[c] Beijing National Laboratory for Molecular Sciences and CAS Research/Education Center of Excellence in Molecular Sciences, Beijing 100190, P. R. China

***Corresponding authors**. E-mails:

liziyu2010@iccas.ac.cn (Z.-Y. L.), shengguihe@iccas.ac.cn (S.-G. H.).

Table of Contents

1 Additional theoretical Methods

Based on the structures calculated at the M06 functional level, the single point energies of reactants and adsorption complexes were recalculated by the high-level partially spin-adapted open-shell coupled-cluster method with single, double, and perturbative triple excitations [RCCSD(T)][1-4] using the Molpro program package.[5] In these CCSD(T) calculations, all the valence electrons were correlated. The basis set used for all atoms were aug-cc-pVDZ and aug-cc-pVTZ (denoted as ADZ and ATZ).[6-8] The two-point complete basis set (CBS) limit extrapolations for total electronic energy were obtained by ADZ/ATZ pair of basis sets (ADZ and ATZ are augmented double-ζ and triple-ζ correlation consistent basis sets, respectively) based on equation 1,[9] which has been recently found to be superior to alternative extrapolation schemes.[10]

$$E_{total,n} = E_{total,CBS} + \frac{A}{(n+1/2)^4} \quad (1)$$

Note that a diagnostic criterion has been examined to evaluate the suitability of single-reference wave function-based methods for $Ta_2D_{2,4}^-$ and products.[11,12]

2 Additional experimental results

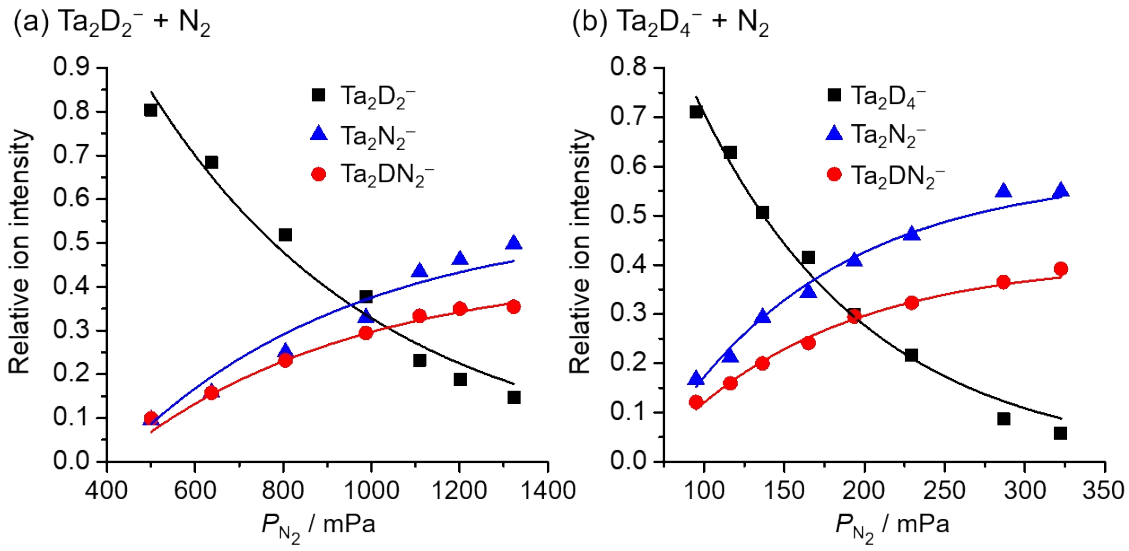

Fig. S1 Variation of ion intensities with respect to the partial pressures of N_2 in the reactions of (a) $Ta_2D_2^-$ and (b) $Ta_2D_4^-$ with N_2. The data points were experimentally measured and the solid lines

were calculated on the basis of rate constants determined form least-squares fitting.

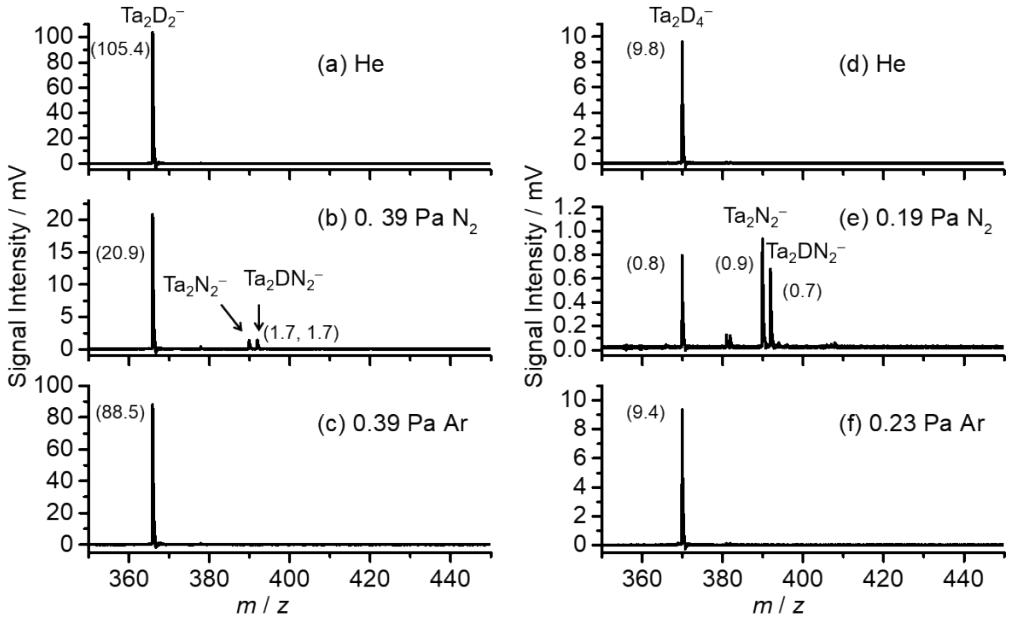

Fig. S2 Time-of-flight mass spectra for the reactions of $Ta_2D_2^-$ cluster anion with (a) He, (b) 0.39 Pa N_2 and (c) 0.39 Pa Ar for about 8.6 ms, the reactions of $Ta_2D_4^-$ cluster anion with (d) He, (e) 0.19 Pa N_2 and (f) 0.23 Pa Ar for about 1.6 ms.

3 Additional theoretical results

3.1 Choice of theoretical methods

Table S1. Experimental and calculated bond dissociation enthalpies [D_0 (A-B) at 0 K, given in eV] of typical diatomic species containing Ta, H, and N atoms as well as the adiabatic electron detachment energy / vertical electron detachment energy (ADE/VDE) of $Ta_2D_2^-$ (given in eV). The standard deviation (σ) of calculated values ($D_{0,\,calc.}$) with respect to experimental data ($D_{0,\,expt.}$) is given.

		D_0(A-B) / eV					$Ta_2D_2^-$		
		Ta-Ta	Ta-N	Ta^+-H	N-N	H-H	ADE	VDE	σ
	Expt.[13]	4.00	6.25	2.35	9.75	4.48	1.51	1.54	
Hybrid Functionals	**M06**	**3.62**	**6.72**	**2.43**	**9.27**	**4.32**	**1.42**	**1.45**	**0.064**
	B3P86	3.44	6.36	2.29	9.78	4.50	1.69	1.73	0.086
	B3LYP	2.86	6.14	2.35	9.60	4.42	1.24	1.27	0.143
	B3PW91	3.31	6.09	2.05	9.43	4.29	1.16	1.18	0.149
	PBE1PBE	3.17	6.00	1.86	9.42	4.16	1.12	1.11	0.184
	B1B95	3.06	6.07	2.07	9.44	4.30	1.06	1.1	0.185
	B1LYP	2.49	5.83	2.53	9.33	4.36	1.08	1.1	0.213
	BMK	2.19	5.99	2.12	9.49	4.29	1.13	0.69	0.289
	M062X	2.46	5.60	2.27	9.44	4.31	0.64	0.64	0.345
Pure Functionals	BP86	4.37	7.03	2.80	10.25	4.50	1.36	1.4	0.107
	BPW91	4.34	6.79	2.45	9.95	4.24	1.18	1.22	0.124
	BLYP	3.72	6.82	2.55	10.09	4.40	1.18	1.21	0.128
	PBEPBE	4.43	7.01	2.62	10.24	4.20	1.22	1.25	0.129
	BPBE	4.39	6.80	2.44	9.95	4.22	1.17	1.2	0.131
	TPSS	4.13	6.63	2.66	9.53	4.54	1.13	1.16	0.144
	M06L	3.84	6.24	2.35	9.41	4.17	1.00	1.04	0.179

3.2 Structural characterization of $Ta_2D_{2,4}^-$

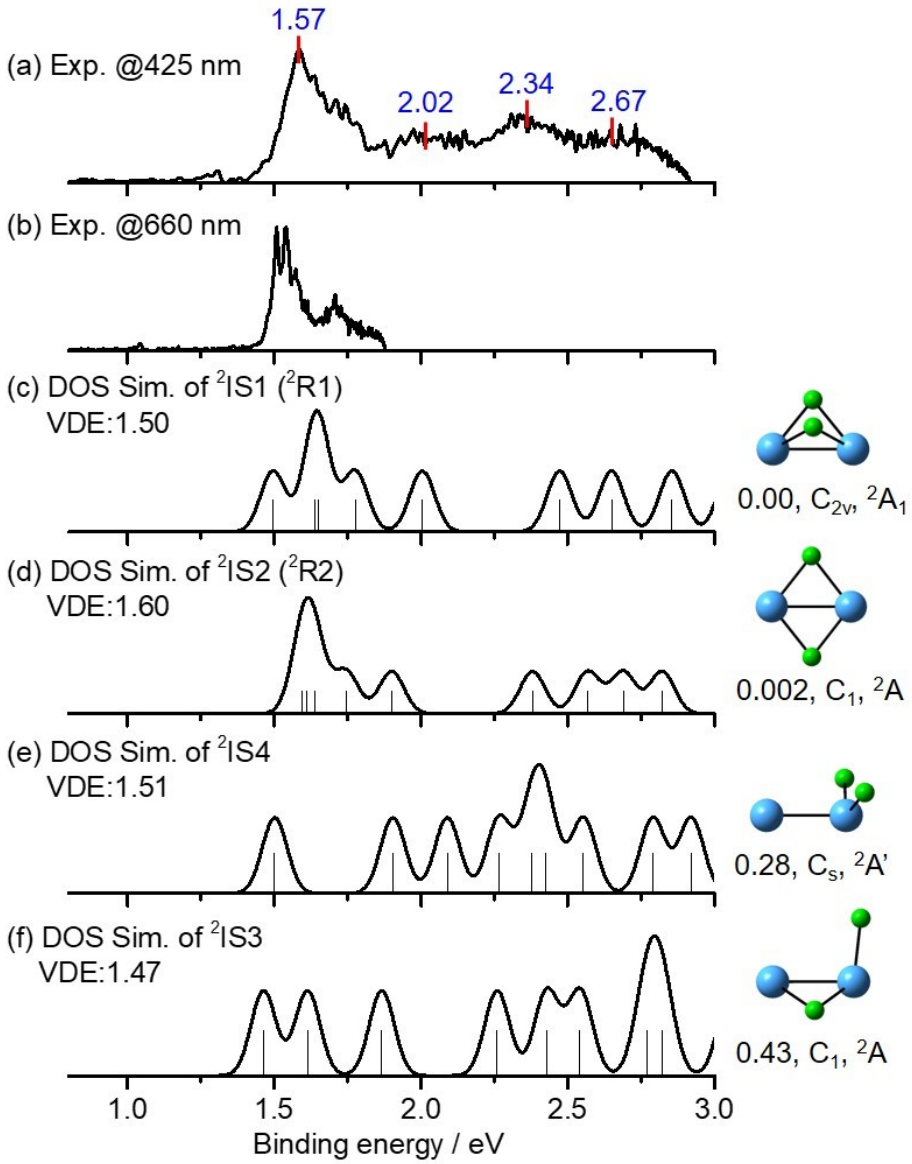

Fig. S3 (a and b) The experimental photoelectron spectra of $Ta_2D_2^-$ at 425 nm and 660 nm, respectively. (c-f) The simulated DOS spectra and structures of the low-lying isomers of $Ta_2D_2^-$. The relative energies with respect to the lowest-lying isomer calculated by RCCSD(T) in unit of eV, the symmetries and the electronic states are listed below the structures. The RCCSD(T)-calculated VDEs are listed in the unit of eV.

The experimental photoelectron spectrum of $Ta_2D_2^-$ recorded with 425 nm photons (Fig. S3a) reveals four major peaks centred at 1.57, 2.02, 2.34, and 2.67 eV, respectively, and the experimental VDE value of $Ta_2D_2^-$ can be determined to be 1.54 eV at a wavelength of 660 nm (Fig. S3b). The RCCSD(T)-calculated VDEs of ^{2}IS1 (^{2}R1 in the main text) and ^{2}IS2 (^{2}R2 in the main text) are 1.50 and 1.60 eV, respectively, which are very close to the experimental value (1.54 eV). In addition, the simulated DOS spectra of ^{2}IS1 and ^{2}IS2 both can resonable reproduce most part of the experimental spectrum (Fig. S3a). The other isomers ^{2}IS3 and ^{2}IS4 can be exclusted due to the obvious high relative energies with respect to the most stable isomer ^{2}IS1 (^{2}IS3: 0.43 eV, ^{2}IS4: 0.28 eV). Therefore, ^{2}IS1 and ^{2}IS2 could be the probable isomers of $Ta_2D_2^-$ generated in experiments.

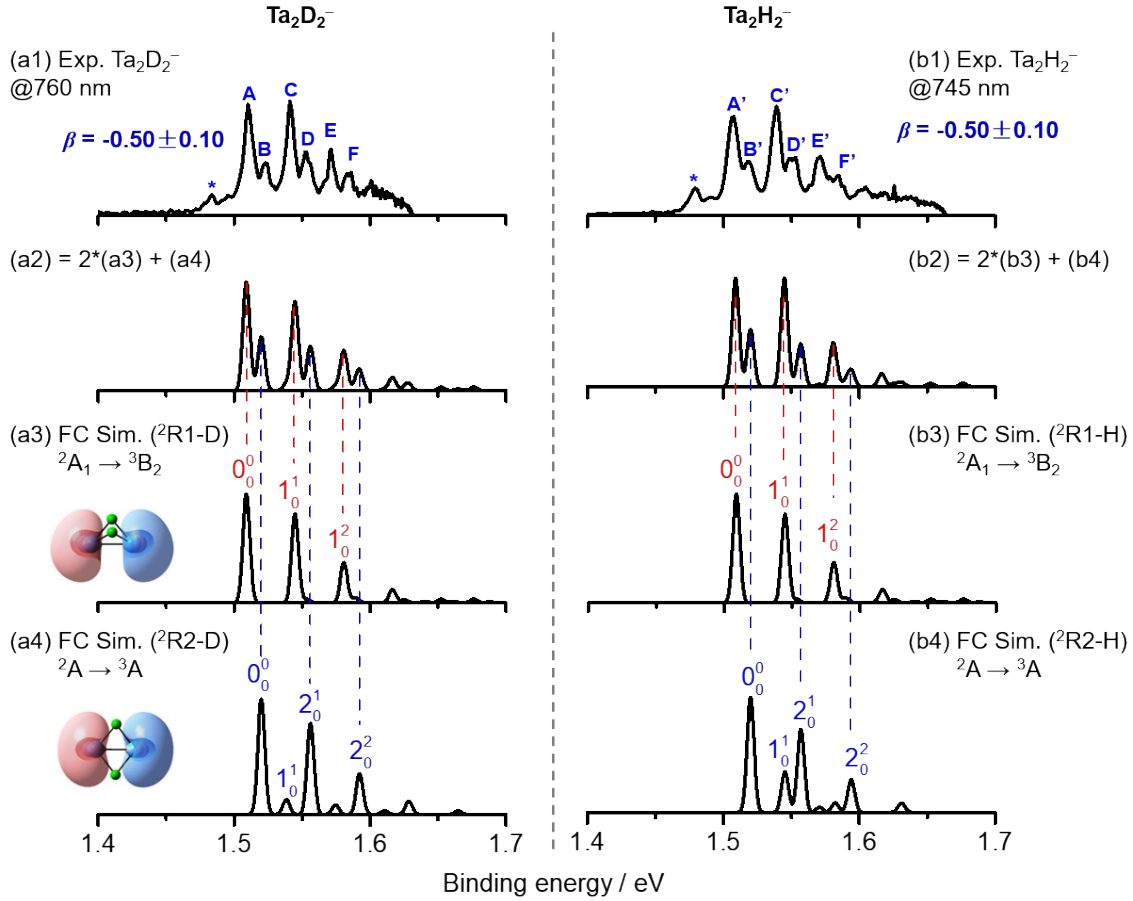

Fig. S4 (a1 and b1) The experimental photoelectron spectra of $Ta_2D_2^-$ at 760 nm and $Ta_2H_2^-$ at 745 nm, respectively. The simulated FC spectra of low-lying isomers of $Ta_2D_2^-$ (a2-a4) and $Ta_2H_2^-$ (b2-b4). The peaks in panels a3, a4, b3, and b4 are red shifted by 0.01 eV, 0.11 eV, 0.01 eV, and 0.11 eV, respectively. The highest occupied molecular orbitals (HOMOs) for each isomer are shown.

Vibrationally resolved detachment spectra for $Ta_2D_2^-$ and $Ta_2H_2^-$ were obtained at the wavelength of 760 nm and 745 nm, repsectively. Note that the peaks labelled with asterisk in Fig. S4 are possibly contributed by the hot bands. Measurement of the photoelectron angular distribution (PAD) of features labeled in Fig. S3a reveals that all transitions fall into one group with the same angular distributions since all the peaks show negative values of the anisotropy parameter ($\beta < 0$), corrpsonding to electron detachment from p or d type atomic orbitals.

DFT calculations predict two low-lying isomers for $Ta_2D_2^-$ (^{2}R1 and ^{2}R2). The Franck-Condon (FC)-simulated spectrum of the $^3B_2 \leftarrow {}^2A_1$ vibrational transition for ^{2}R1 can reproduce the three strong vibrationally resolved peaks (A, C, and E) in the experimental spectrum, corresponding to a stretching vibration of the two Ta atoms (υ_1, ~289 cm^{-1}). Besides, the calculated results show that a low-lying isomer of $Ta_2D_2^-$ (^{2}R2) with 0.002 eV higher than the ground state structure (^{2}R1) has a similar FC simulated spectrum that can contribute to the remainder of the experimental spectrum (B, D, and F). The FC simulated spectrum of ^{2}R2-D ($Ta_2D_2^-$, Fig. S4a4) contains a dominant progression from the Ta-Ta stretching mode (υ_2, 290 cm^{-1}) modulated by a weak progression for the wagging mode of two D atoms (υ_1, ~145 cm^{-1}). For ^{2}R2-H ($Ta_2H_2^-$, Fig. S4b4), the frequency of the wagging mode of two D atoms changes to 202 cm^{-1}. Note that the major progressions all come from the Ta-Ta stretching, as a result, the isotopic labelling would not influence the experimental results, which rationalizes the almost same spectra for $Ta_2D_2^-$ (Fig. S4a1) and $Ta_2H_2^-$ (Fig. S4b1).

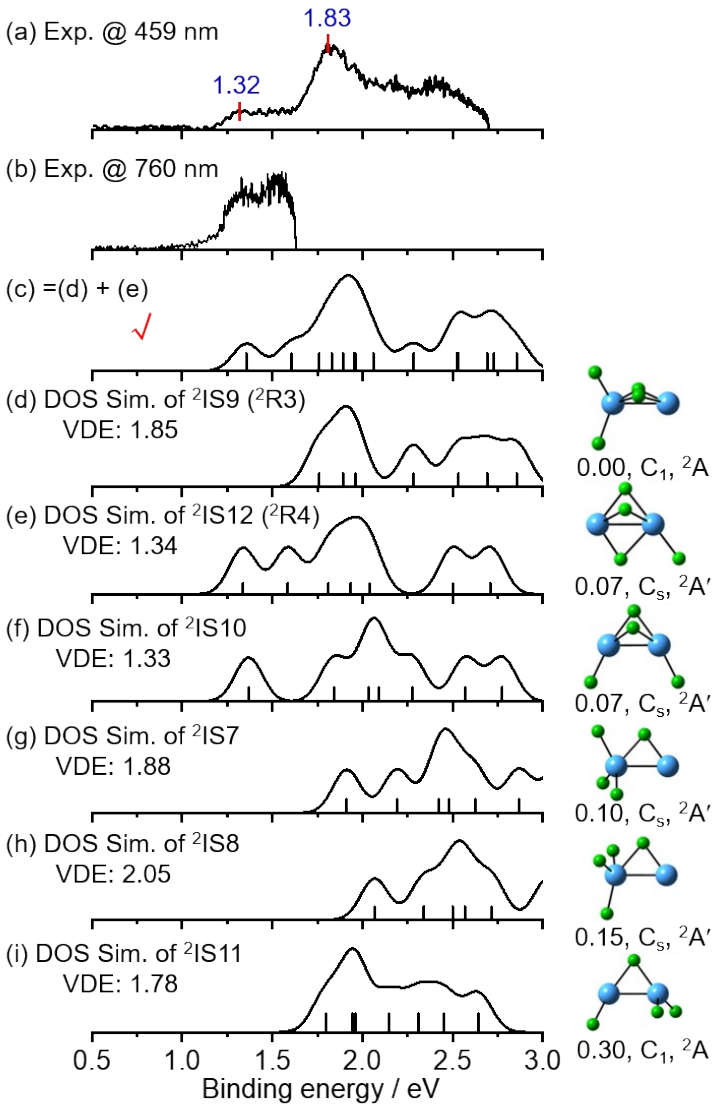

Fig. S5 (a and b) The experimental photoelectron spectra recorded with 459 nm and 760 nm laser excitations at 10 K for $Ta_2D_4^-$, respectively. (c-i) The simulated density-of-state (DOS) spectra and structures of the low-lying isomers of $Ta_2D_4^-$. The simulated DOS spectrum of ^{2}R3 is red shifted by 0.08 eV. The relative energies with respect to the lowest-lying isomer calculated by RCCSD(T) in unit of eV, the symmetries and the electronic states are listed below the structures. The RCCSD(T)-calculated VDEs are listed in the unit of eV.

For $Ta_2D_4^-$, two broad bands centred at 1.32 eV and 1.83 eV are present at 459 nm excitation (Fig. S5a). The calculated lowest-lying isomer ^{2}IS9 (^{2}R3 in the main text) of $Ta_2D_4^-$ features two bridging D atoms and two terminal D atoms. The DOS-simulated spectrum of ^{2}IS9 (Fig. S5d) can reasonably reproduce the experimental spectrum from 1.50 to 2.75 eV, and the calculated VDE of ^{2}IS9 is close to the experimental value (1.85 eV *vs* 1.83 eV), suggesting that the ^{2}IS9 is the most probable species of $Ta_2D_4^-$ generated in the experiment. In addition, the simulated spectrum of the low-lying isomer ^{2}IS12 (^{2}R4 in the main text) with three bridging D atoms and one terminal D atom (Fig. S5e) can well reproduce the two bands around over the range of 1.0~1.6 eV in the experimental spectrum recorded at 760 nm (Fig. S5b) in terms of VDE (1.34 eV *vs* 1.32 eV) and spectral patterns. Therefore, both ^{2}IS9 and ^{2}IS12 may contribute to the $Ta_2D_4^-$ species in experiments.

3.3 Structural isomers of $Ta_2D_{2,4}^-$, $Ta_2N_2^-$, $Ta_2DN_2^-$, and $Ta_2D_{2,4}N_2^-$

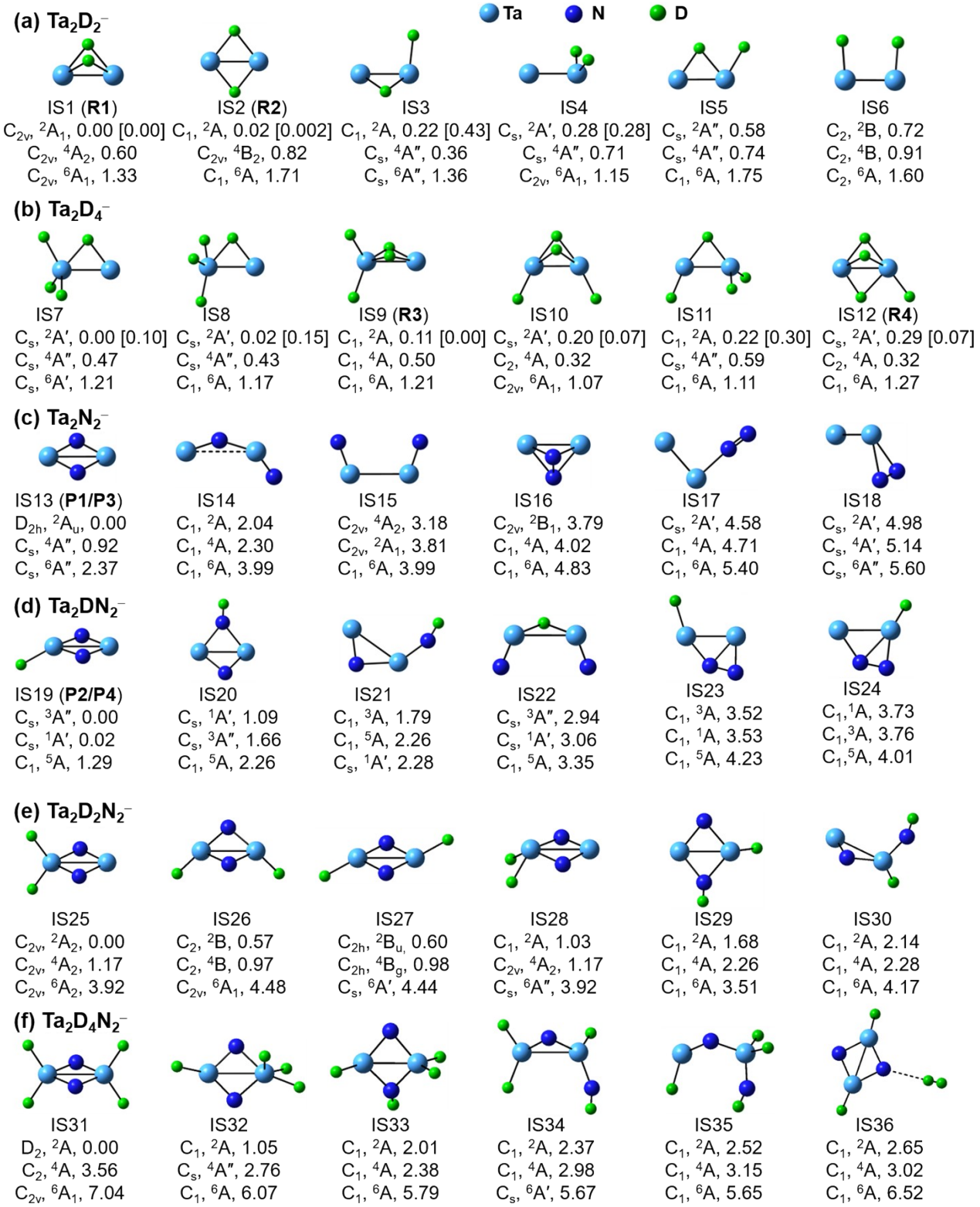

Fig. S6 DFT calculated isomers for $Ta_2D_2^-$ (a), $Ta_2D_4^-$ (b), $Ta_2N_2^-$ (c), $Ta_2DN_2^-$(d), $Ta_2D_2N_2^-$ (e) and $Ta_2D_4N_2^-$ (f). The relative energies (ΔH_0, in eV) with respect to the lowest-lying isomers are given below the structures. The RCCSD(T)-calculated relative energies are given in brackets.

3.4 Reaction mechanisms of $Ta_2D_2^-$ (^{2}R1/^{2}R2) +N_2

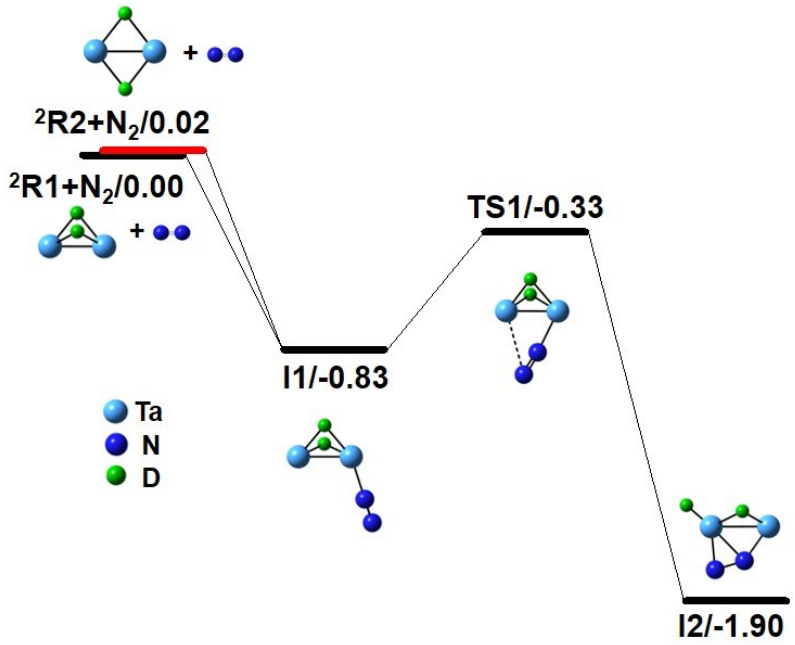

Fig. S7 The potential energy surface of ^{2}R1/^{2}R2 + N_2. The zero-point vibration corrected energies of intermediates (I*n*) and transition states (TS*n*) relative to the separated reactants (^{2}R1 + N_2) are in eV.

3.5 Reaction mechanisms of $Ta_2D_4^-$ (^{2}R3/^{2}R4) +N_2

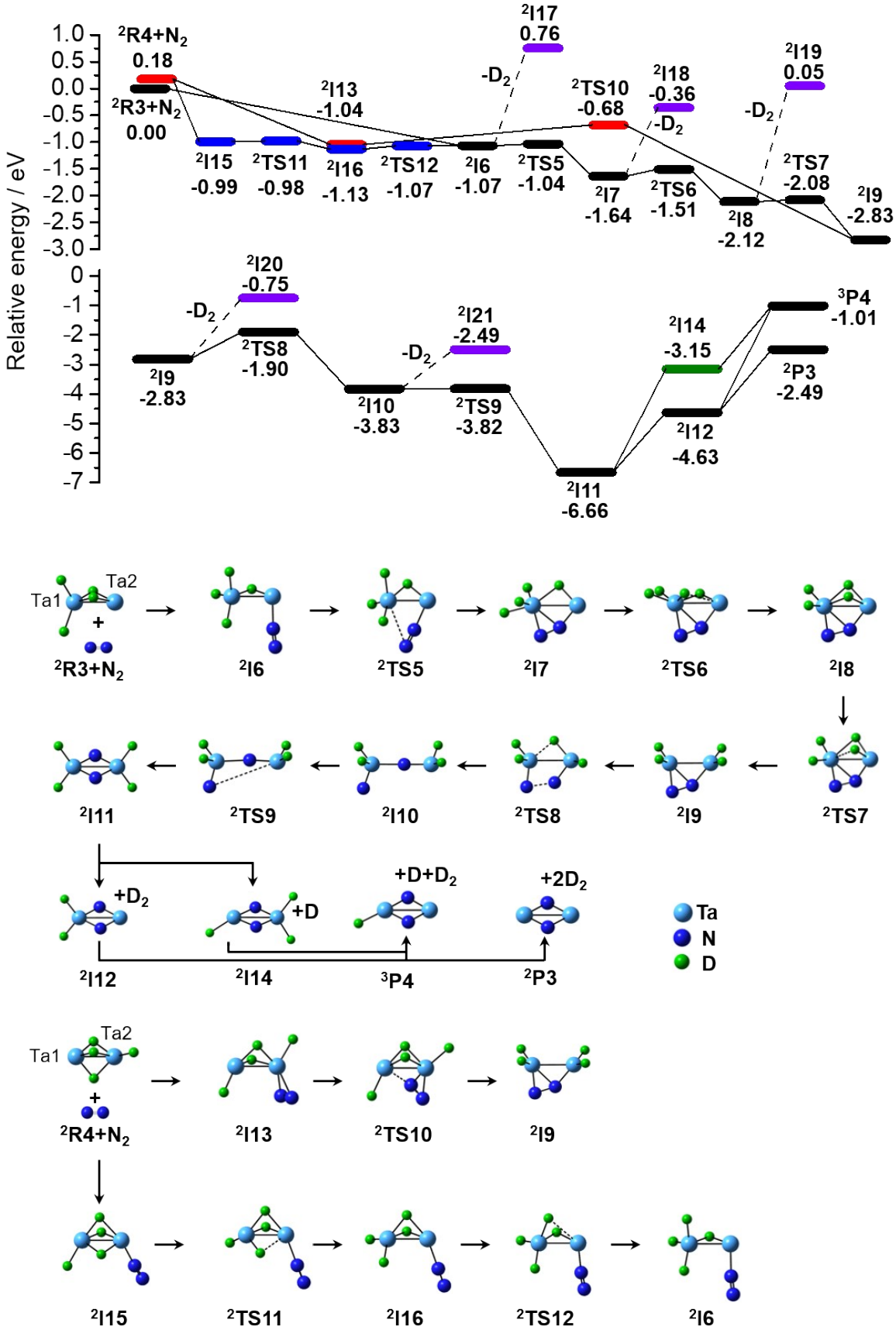

Fig. S8 The potential energy surface of ^{2}R3/^{2}R4 + N_2. The zero-point vibration corrected energies of intermediates (I*n*) and transition states (TS*n*) relative to the separated reactants (^{2}R3 + N_2) are in eV.

3.6 Potential energy profiles for the isomerization of ^{2}R1 → ^{2}R2 of $Ta_2D_2^-$ and ^{2}R3 → ^{2}R4 of $Ta_2D_4^-$

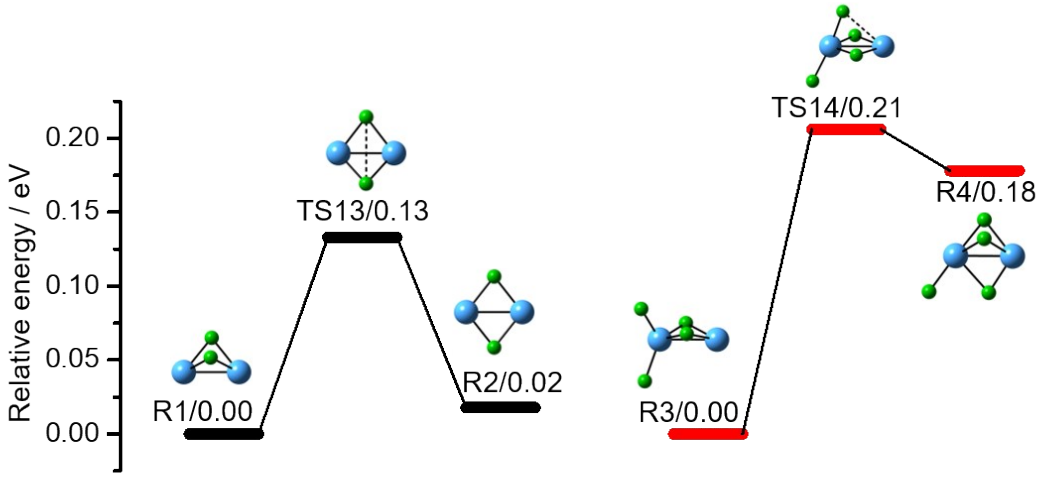

Fig. S9 The DFT-calculated potential energy profiles for the isomerization of ^{2}R1 → ^{2}R2 of $Ta_2D_2^-$ and ^{2}R3 → ^{2}R4 of $Ta_2D_4^-$. The relative energies with respect to lowest-lying isomer are given in eV.

3.7 The calculated VDEs and the binding energy of N_2 of all intermediates

Table S2. The calculated VDEs and the binding energy of N_2 of all intermediates on the potential energy profile for the reaction of $Ta_2D_2^- + N_2$ and $Ta_2D_4^- + N_2$.

isomer	VDE (eV)	The binding energy of N_2 (eV)
I1	1.63	0.83
I2	1.84	1.90
I3	1.57	2.03
I4	3.45	3.80
I5	1.47	5.93
I6	1.83	1.07
I7	2.64	1.64
I8	1.86	2.12
I9	2.37	2.83
I10	3.72	3.83
I11	1.53	6.66

3.8 Molecular orbital analysis of $Ta_2D_2^-$ and $Ta_2D_4^-$

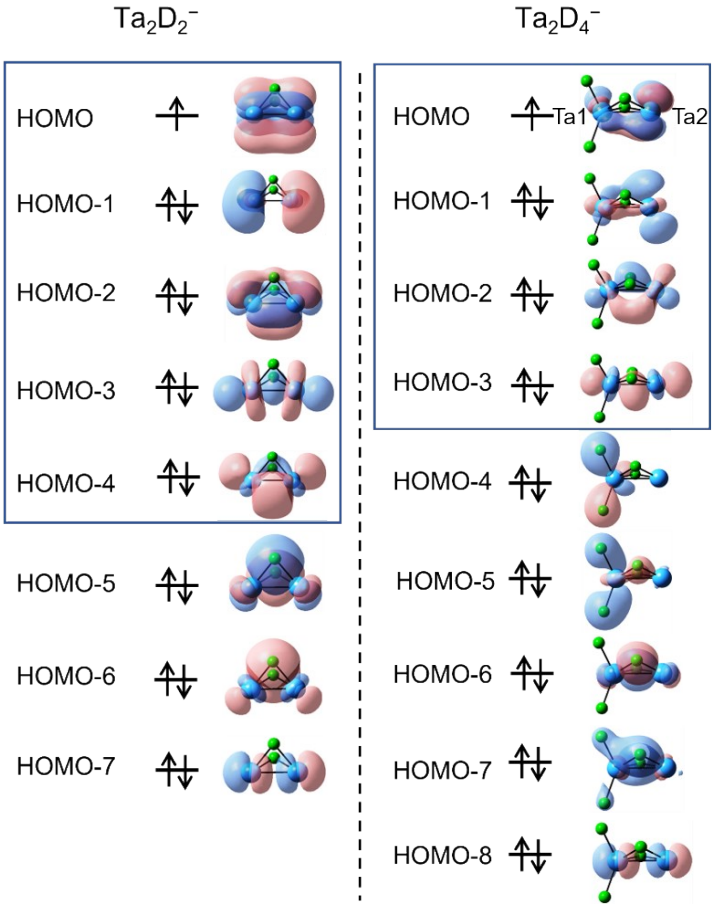

Fig. S10 Molecular orbital analysis of $Ta_2D_2^-$ and $Ta_2D_4^-$. The up and down arrows denote α and β electrons.

The molecular orbital analysis was carried out and the result was added as Fig. S10. Five occupied molecular orbitals (HOMO to HOMO-4) are composed of s/d atomic orbitals of Ta in $Ta_2D_2^-$. When the two additional D atoms bond with $Ta_2D_2^-$ to form $Ta_2D_4^-$, two electrons from the occupied MO pair with the single electrons from D atoms to form two new Ta-D bonds (HOMO-4 and HOMO-5 in $Ta_2D_4^-$). In addition, two of the five MOs (HOMO-2 and HOMO-3 in $Ta_2D_4^-$) almost remain unchanged upon the D atoms bonding. While the first two MOs (HOMO and HOMO-1) rearrange upon the D atom addition with the electron densities around Ta1 shifting to Ta2 atom. As a result, the electron densities are more localized on Ta2 atom in $Ta_2D_4^-$ than that in $Ta_2D_2^-$, which plays a vital role to facilitate the approaching of N_2 towards Ta2 as well as to maximize the overlap between the occupied MO in $Ta_2D_4^-$ and the empty MO in N_2, as shown in Figs. 4 and 5 in the main text.

4 References

1 G. D. Purvis III and R. J. Bartlett, *J. Chem. Phys.*, 1982, **76**, 1910-1918.

2 K. Raghavachari, G. W. Trucks, J. A. Pople and M. Head-Gordon, *Chem. Phys. Lett.*, 1989, **157**, 479-483.

3 J. D. Watts, J. Gauss and R. J. Bartlett, *J. Chem. Phys.*, 1993, **98**, 8718-8733.

4 P. J. Knowles, C. Hampel and H. J. Werner, *J. Chem. Phys.*, 1993, **99**, 5219-5227.

5 H. J. Werner, P. J. Knowles, R. Lindh, F. R. Manby, M. Schutz, P. Celani, T. Korona, A. Mitrushenkov, G. Rauhut, T. B. Adler, R. D. Amos, A. Bernhardsson, A. Berning, D. L. Cooper, M. J. O. Deegan, A. J. Dobbyn, F. Eckert, E. Goll, C. Hampel, G. Hetzer, T. Hrenar, G. Knizia, C. Koppl, Y. Liu, A. W. Lloyd, R. A. Mata, A. J. May, S. J. McNicholas, W. Meyer, M. E. Mura, A. Nicklass, P. Palmieri, K. Pfluger, R. Pitzer, M. Reiher, U. Schumann, H. Stoll, A. J. Stone, R. Tarroni, T. Thorsteinsson, M. Wang and A.Wolf, MOLPRO, version 2010.1 A Package of ab initio Programs, See http://www.molpro.net.

6 R. A. Kendall, T. H. Dunning Jr. and R. J. Harrison, *J. Chem. Phys.*, 1992, **96**, 6796-6806.

7 T. H. Dunning Jr., *J. Chem. Phys.*, 1989, **90**, 1007-1023.

8 N. B. Balabanov and K. A. Peterson, *J. Chem. Phys.*, 2005, **123**, 064107.

9 J. M. L. Martin, *Chem. Phys. Lett.*, 1996, **259**, 669-678.

10 D. Feller, K. A. Peterson and J. G. Hill, *J. Chem. Phys.*, 2011, **135**, 044102.

11 T. J. Lee and P. R. Taylor, *Int. J. Quantum Chem.*, 1989, **36**, 199-207.

12 S. R. Langhoff and E. R. Davidson, *Int. J. Quantum Chem.*, 1974, **8**, 61-72.

13 Y. R. Luo, *Comprehensive Handbook of Chemical Bond Energies.* CRC Press: Boca Raton, FL, 2007.